Thermochimica Acta, 129 (1988) 309–324
Elsevier Science Publishers B.V., Amsterdam – Printed in The Netherlands

CALORIMETRIC DETERMINATION OF PURITY BY SIMULATION OF DSC CURVES

S. SARGE, S. BAUERECKER and H.K. CAMMENGA

Institut für Physikalische und Theoretische Chemie der Technischen Universität Braunschweig, Hans-Sommer-Straße 10, D-3300 Braunschweig (F.R.G.)

(Received 29 September 1987)

ABSTRACT

A method of purity determination by differential scanning calorimetry is described which is not restricted to eutectic systems or small impurity concentrations. This method is based on direct comparison between the measured melting curve and a calculated curve which is obtained with a simple R–C model of a heat flux calorimeter. First results show that the error is in the order of 10% of the impurity concentration.

INTRODUCTION

The calorimetric determination of purity by quantitative analysis of the fusion peak obtained with a differential scanning calorimeter is common practice in science and industry. The hitherto used methods of evaluation are based on equilibrium thermodynamics and do not take into account temperature gradients in the system caused by the dynamic increase in the oven temperature. In addition, the methods of evaluation are restricted to eutectic systems and to small concentrations of impurities. With uncritical application of the evaluation method, i.e. for systems for which it has not been optimized, errors of the same magnitude as the impurity concentration itself may occur.

In this study a method will be described which allows calorimetric purity analysis over the whole concentration range of the phase diagram for eutectic systems, systems with mixed crystals, and others.

CLASSICAL METHODS OF PURITY ANALYSIS

The basis of the classical methods of calorimetric purity analysis is the thermodynamic description of the isobaric melting of a two-component

---

This paper was presented at the J.C.A.T., Ferrara, Italy, October 1986.

0040-6031/88/$03.50

mixture with complete miscibility in the liquid phase, immiscibility in the solid phase, and the formation of a eutectic or eutectics. In this case the coexistence of solution (melt) and crystals is expressed by [1]

$$\int_1^{a_{X_1}} \mathrm{d}\ln(a_{X_1}) = \int_{T_{\mathrm{fus}}}^{T} \frac{\Delta_{\mathrm{fus}}H_1}{RT^2}\,\mathrm{d}T \tag{1}$$

(The meaning of the symbols is explained below.)

After introduction of the following simplifications and integration one obtains the law of van 't Hoff for freezing point depression

$$\mathrm{d}(a_{X_1})/\mathrm{d}T \simeq 0 \tag{2}$$

$$\mathrm{d}(\Delta_{\mathrm{fus}}H_1^{\ominus})/\mathrm{d}T \simeq 0 \tag{3}$$

$$a_{X_1} \simeq X_1 \tag{4}$$

$$\ln(X_1) = \ln(1 - X_2) \simeq -X_2 \tag{5}$$

$$T_{\mathrm{fus}}T \simeq T_{\mathrm{fus}}^2 \tag{6}$$

$$X_2 = \sum_{i=2}^{k} X_i \tag{7}$$

$$X_2 = \left(\frac{\Delta_{\mathrm{fus}}H_1^{\ominus}}{R}\right)\left(\frac{\Delta T}{T_{\mathrm{fus}}^2}\right) \tag{8}$$

$$T = T_{\mathrm{fus}} - \left(\frac{RT_{\mathrm{fus}}^2}{\Delta_{\mathrm{fus}}H_1^{\ominus}}\right)X_2 \tag{9}$$

With the simplifications used it is usually agreed that the applicability of eqn. (9) is restricted to the range $X_2 < 0.05$.

An assessment of the influence of the simplifications used by means of thermodynamic data for eqns. (2), (3) and (4) and of mathematical estimations for eqns. (5) and (6) valid for a representative number of organic and inorganic substances shows that the simplifications introduced may already cause a relative error $(X_{\mathrm{real}} - X_{\mathrm{exp}})/X_{\mathrm{real}}$ of the same magnitude as the concentration of the impurities.

The fusion temperature as a function of the fraction melted in the mixture is described by

$$T = T_{\mathrm{fus}} - \left(\frac{RT_{\mathrm{fus}}^2}{\Delta_{\mathrm{fus}}H_1^{\ominus}}\right)X_2^{\star}\left(\frac{1}{F}\right) \tag{10}$$

A plot of T vs. $1/F$ should yield a straight line with intercept T_{fus} and slope $-RT_{\mathrm{fus}}^2X_2^{\star}/\Delta_{\mathrm{fus}}H_1^{\ominus}$.

In reality, however, one normally obtains a concave curve. Reasons for this are, inter alia, thermodynamic non-equilibrium in the sample, thermal

gradients in the instrument and within the sample, existence of mixed crystals, and undetected beginning of melting caused by the limited sensitivity of the calorimeter.

Usually, the calorimetric purity determination consists of the following steps:

1. Determination of the fusion curve (sample mass, a few milligrams; heating rate, ~ 1 K min^{-1}).
2. Correction of the curve with respect to temperature and calorimetric calibration of the instrument.
3. Determination of the fractions melted F_i in the mixture during melting (sometimes after deconvolution of the curve) and determination of the corresponding temperatures T_i (sometimes after correction with the heat resistance).
4. Linearization of the $T_i = T_i\ (1/F_i)$ plot by one of several methods in different ranges of $1/F$ $(2 < (1/F) < 50)$. Normally this is done by finding the best value of K, which compensates the undetermined part of the heat of fusion between the eutectic temperature and the observed peak onset

$$\frac{1}{F_i} = \frac{\sum_{n=0}^{\infty} \left((\mathrm{d}H_n/\mathrm{d}t)\ \Delta t\right) + K}{\sum_{n=0}^{i} \left((\mathrm{d}H_n/\mathrm{d}t)\ \Delta t\right) + K} \tag{11}$$

5. Evaluation of T_{fus} and $X_2^{\star}$ from the intercept and slope of the linearized curve.

An enormous number of papers has been published on the influence of different experimental and computational factors (sample mass, method of sample preparation, history of sample, purity, type of phase diagram, heating rate, determination of fractions melted, method of linearization, range of linearization, etc.). The result is that an accuracy of better than 10% can be obtained only after calibration of the DSC instrument with similar systems (see refs. 2–4, for example).

The DSC instrument causes an important source of error in blurring the signal produced by the sample (the enthalpy production) and the heat flux measured between sample and reference crucible. Only in a few cases has this effect been taken into account by applying a method of deconvolution.

A systematic evaluation and quantitative analysis of the parameters mentioned is difficult, because the quantitative determination of these conditions and their systematic variation causes considerable experimental problems. A mathematical model of a heat flux DSC is developed below which allows simulation of DSC curves. This method demonstrates the influence of a variation in the parameters of the instrument and the sample on the shape of the DSC curve, and on the apparent purity determined.

MATHEMATICAL MODELLING OF A HEAT FLUX CALORIMETER

The experiments were performed using a Heraeus TA 500 dynamic heat flux DSC. In this instrument a cylindrical silver oven surrounds a rectangular plate of aluminium oxide, which carries two vapour-deposited Pt 100 resistance thermometers (see Fig. 1). The sample temperature is determined by measuring the resistance below the sample crucible. The sensitivity of the instrument is approx. 17 μV mW^{-1}, the resolution of the connected digital voltmeters is 0.1 μV for the temperature difference and 0.01 K for the absolute temperature.

On the one hand the mathematical model of this calorimeter must be able to describe the essential properties of the instrument, and on the other hand it has to be simple enough to allow its application in practice. For this purpose the calorimeter has been subdivided into several zones of equal temperature (see Fig. 2). Each zone consists of a definite heat capacity and is connected with the neighbouring zones by localized heat resistances.

This model can be reduced to a simple R–C model (see Fig. 3) and can be described by a system of four coupled differential equations. If the calorimeter equations $\Delta T = R(\mathrm{d}Q/\mathrm{d}t)$ and $(\mathrm{d}T/\mathrm{d}t) = (1/C)\,(\mathrm{d}Q/\mathrm{d}t)$ are valid one obtains

$$\frac{\mathrm{d}Q_1}{\mathrm{d}t} = \frac{1}{R_1}(T_0 - T_1) + \frac{1}{R_4}(T_2 - T_1) \tag{12}$$

$$\frac{\mathrm{d}Q_2}{\mathrm{d}t} = \frac{1}{R_2}(T_0 - T_2) + \frac{1}{R_3}(T_3 - T_2) + \frac{1}{R_4}(T_1 - T_2) \tag{13}$$

$$\frac{\mathrm{d}Q_3}{\mathrm{d}t} = \frac{1}{R_3}(T_2 - T_3) \tag{14}$$

$$\frac{\mathrm{d}T_0}{\mathrm{d}t} = \beta(\text{heating rate}) \tag{15}$$

$$\frac{\mathrm{d}T_1}{\mathrm{d}t} = \left(\frac{1}{C_1}\right)\left(\frac{\mathrm{d}Q_1}{\mathrm{d}t}\right) = \frac{1}{R_1C_1}(T_0 - T_1) + \frac{1}{R_4C_1}(T_2 - T_1) \tag{16}$$

$$\frac{\mathrm{d}T_2}{\mathrm{d}t} = \left(\frac{1}{C_2}\right)\left(\frac{\mathrm{d}Q_2}{\mathrm{d}t}\right) = \frac{1}{R_2C_2}(T_0 - T_2) + \frac{1}{R_3C_2}(T_3 - T_2) + \frac{1}{R_4C_2}(T_1 - T_2) \tag{17}$$

$$\frac{\mathrm{d}T_3}{\mathrm{d}t} = \frac{1}{C_3}\left[\frac{\mathrm{d}Q_3}{\mathrm{d}t} - \frac{\mathrm{d}H}{\mathrm{d}t}\right] = \frac{1}{R_3C_3}(T_2 - T_3) - \left(\frac{1}{C_3}\right)\left(\frac{\mathrm{d}H}{\mathrm{d}t}\right) \tag{18}$$

As a consequence of the enthalpy production of the sample $(\mathrm{d}H/\mathrm{d}t)$, the non-linear system of equations can only be solved numerically (method of Runge-Kutta).

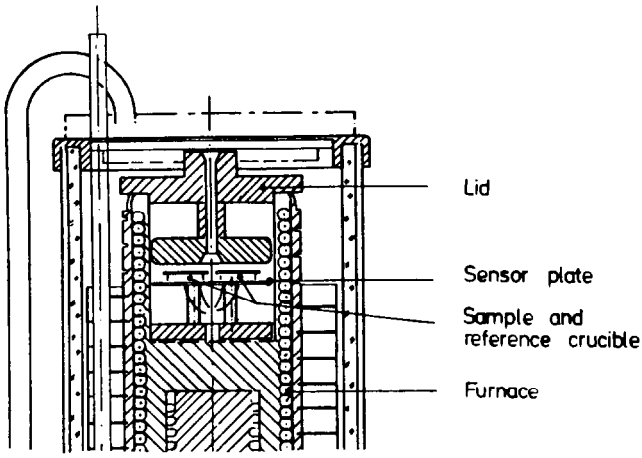

Fig. 1. Cross-sectional view of the Heraeus TA 500 instrument.

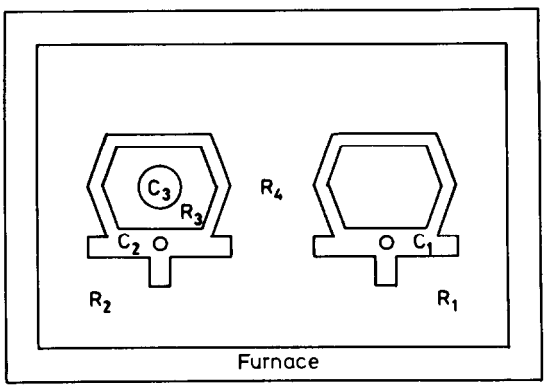

Fig. 2. Zones of equal temperature in the calorimeter model.

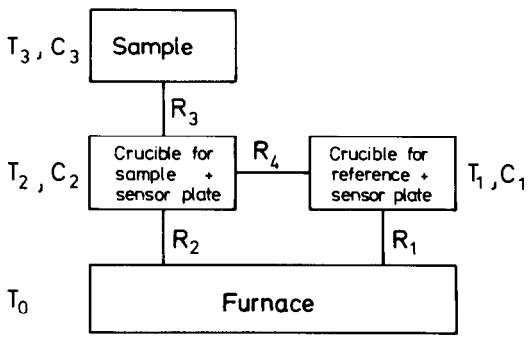

Fig. 3. The reduction of the calorimeter to a R–C model.

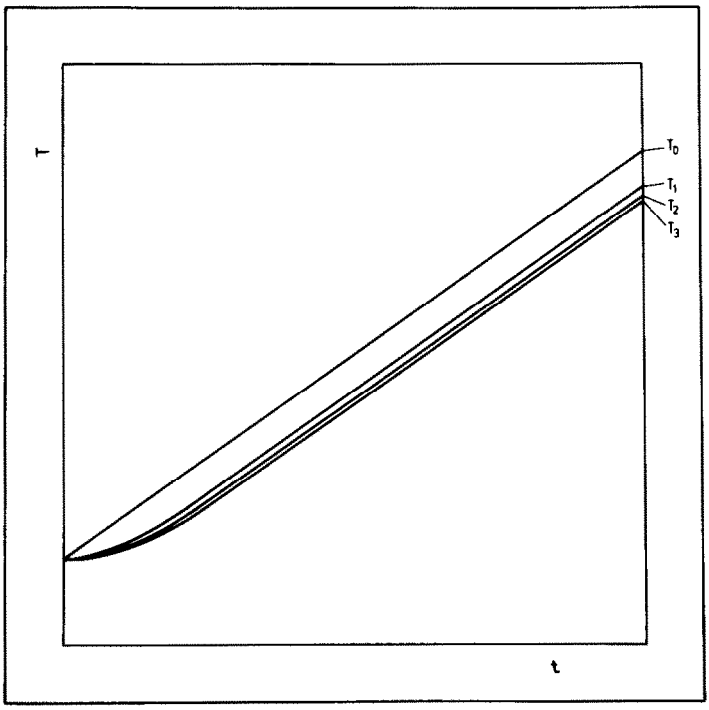

Fig. 4. Temperature dependence T_0, T_1, T_2 and T_3 (not to scale). $T_0 - T_1$ $(t \to \infty) = 0.9872$ K; $T_1 - T_2$ $(t \to \infty) = 0.0158$ K; $T_2 - T_3$ $(t \to \infty) = 0.0049$ K; $\beta = 1$ K min^{-1}.

The parameters R_1, C_1, R_2, C_2 and R_4 can be obtained by analytical solution for the special case $(\mathrm{d}H/\mathrm{d}t) = 0$ and $t \to \infty$

$$T_2 - T_1 = \frac{\beta R_4 (R_1 C_1 - R_2 C_3 - R_2 C_2)}{R_1 + R_2 + R_4} \tag{19}$$

$$T_0 - T_2 = \frac{\beta R_2 (R_1 C_1 + R_1 C_2 + R_4 C_2 + R_4 C_3 + R_1 C_3)}{R_1 + R_2 + R_4} \tag{20}$$

With $R_1 = R_2$ and $C_1 = C_2$ (symmetric properties of the calorimeter) we have

$$T_2 - T_1 = -\beta R_4 \left(\frac{R_1 C_3}{R_4 + 2R_1} \right) \tag{21}$$

$$T_0 - T_2 = \beta R_1 \left[C_1 + C_3 \frac{R_1 + R_4}{R_4 + 2R_1} \right] \tag{22}$$

$$T_2 - T_3 = \beta R_3 C_3 \tag{23}$$

TABLE 1

Parameters of the model of the Heraeus TA 500 calorimeter

	Using C_p-measurement	After optimization
C_1	0.128 J K^{-1}	0.128 J K^{-1}
C_2	0.128 J K^{-1}	0.142 J K^{-1}
R_1	391 K W^{-1}	391 K W^{-1}
R_2	391 K W^{-1}	391 K W^{-1}
R_3	–	60–110 K W^{-1}
R_4	108 K W^{-1}	98 K W^{-1}
β	1 K min^{-1}	0.98 K min^{-1}

Figure 4 shows the dependence of T_0, T_1, T_2 and T_3 under these conditions.

The parameters R_1, C_1, R_2, C_2 and R_4 can be determined from the temperature differences $T_2 - T_1$ and $T_0 - T_2$ in performing two DSC measurements, one with $C_3 = 0$ (empty sample container) and the other with $C_3 \neq 0$ (preferentially with a high sample mass), under otherwise identical experimental conditions. Since C_3 is known from the mass and specific heat capacity of the sample, only R_3 must be estimated from properties of the sample, the instrument and the constructional materials. In an alternative, complementary method one fits a calculated curve to a simulated one by variation of the parameters. Table 1 shows the results for the Heraeus TA 500 calorimeter. The left column shows the data obtained by two successive measurements, one with "sapphire" (α-Al_2O_3) and the other with two empty containers. The right column gives the data obtained by optimization.

The second method yields different values for C_1 and C_2 (or for R_1 and R_2, because the simulation only involves the products R_1C_1 and R_2C_2). This indicates an asymmetry of the calorimeter used. Furthermore, but not yet considered, the parameters are functions of temperature and heating rate.

THE ENTHALPY PRODUCTION OF THE SAMPLE

For the calculation of the fusion curve the van 't Hoff equation has been used without the simplifications of eqns. (5) and (6)

$$\ln(1 - X_2) = -\left(\frac{\Delta_{fus}H_1^{\ominus}}{R}\right)\left(\frac{T_{fus} - T}{T_{fus}T}\right) \tag{24}$$

The enthalpy $H = H(T)$ of the sample is expressed by

$$H(T) = F(T)\left(\Delta_{fus}H_1^{\ominus}\right) \tag{25}$$

$$F(T) = \frac{n_{1,\mathrm{lq}} + n_2}{n_1 + n_2} = \frac{X_2^{\star}}{X_2(T)} \tag{26}$$

$$\frac{\mathrm{d}H}{\mathrm{d}t} = \left(\frac{\mathrm{d}H}{\mathrm{d}T}\right)\left(\frac{\mathrm{d}T}{\mathrm{d}t}\right) = X_2^{\star}\left(\frac{\Delta_{\mathrm{fus}}H_1^{\ominus 2}}{RT^2}\right) \times \frac{\exp\left[-\dfrac{\Delta_{\mathrm{fus}}H_1^{\ominus}(T_{\mathrm{fus}} - T)}{RT_{\mathrm{fus}}T}\right]}{\left[1 - \exp\left[-\dfrac{\Delta_{\mathrm{fus}}H_1^{\ominus}(T_{\mathrm{fus}} - T)}{RT_{\mathrm{fus}}T}\right]\right]^2}\left(\frac{\mathrm{d}T}{\mathrm{d}t}\right) \tag{27}$$

The enthalpy production of the eutectic has been calculated with the assumptions $\Delta_{\mathrm{fus}}H_1 = \Delta_{\mathrm{fus}}H_2 = \Delta_{\mathrm{fus}}H$ and $\Delta_{\mathrm{mix}}H = 0$ according to

$$H_{\mathrm{eu}} = \left(\frac{n_2 + n_{\mathrm{eu}}}{n_1 + n_2}\right)\Delta_{\mathrm{fus}}H = \left(\frac{X_2^{\star}}{X_{\mathrm{eu}}}\right)\Delta_{\mathrm{fus}}H = \int_0^{T_{\mathrm{eu}}}\left(\frac{\mathrm{d}H}{\mathrm{d}T}\right)\mathrm{d}T \tag{28}$$

In additon, a form factor Z has been introduced into the calculation which takes into account the inhomogeneous temperature distribution within the sample. This form factor does not affect the initial melting range

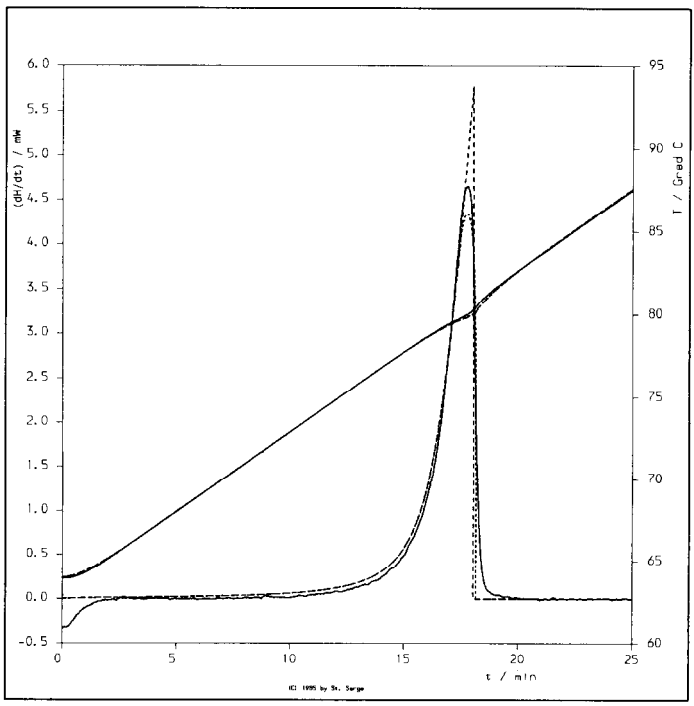

Fig. 5. Enthalpy production of 3.55 mg naphthalene contaminated with 0.98 mol% *trans*-azobenzene. Heating rate, 1 K min^{-1}; ———, experimental curve; — — —, according to eqn. (27); · · · · · ·, corrected with the form factor.

(important for purity analysis): Z only gives a better fit with reality of the peak maximum and the decay part of the melting peak. For metals, the value of Z is close to unity, for organic samples it is between 0.5 and 0.8.

The enthalpy production of the sample can be fitted to any physical or chemical process. Thus it is possible to calculate DSC curves, inter alia, for eutectic systems ($0 < X_2^\star < 1$), systems with mixed crystals ($0 < X_2^\star < 1$), and complex processes, e.g. melting with simultaneous decomposition of the melt (thermally labile compounds).

Figure 5 shows the enthalpy production of a sample of 3.55 mg naphthalene, "contaminated" with 0.98 mol% *trans*-azobenzene together with the curve calculated using eqn. (27) and the experimental curve.

COMPUTER

The simulations of the DSC curves were performed at the computer centre of the Technical University of Brunswick (computer: Amdahl 470 V/7 (ca. 5 MIPS), operating system: VM/SP (IBM)). The programs were written in FORTRAN-77 (FORTRAN/VS, IBM) using NAGF- and GHOST-80 subroutines. The necessary CPU time is 2–5 s. A similar calculation with an IBM-XT personal computer (operating system: PC-DOS 3.20, compiler: PROFESSIONAL FORTRAN) needs 2–5 min. (Further information is available via the network EARN, I3041201 at DBSTU1.)

INFLUENCE OF PROPERTIES OF THE HERAEUS CALORIMETER AND THE SAMPLE ON THE SHAPE OF THE DSC CURVE

Simulation of DSC curves (see Figs. 6–12) allows illustration of the influence of various properties of the calorimeter and the materials on the DSC curve. This technique shows that changes of some parameters (or combinations of parameters) have the same influence on the shape of the DSC curve as the impurity concentration itself.

In Figs. 6–12 the respective parameter is varied by the factor 3 (with the exception of Fig. 11). The medium curve is always identical and shows the calculated DSC curve of a sample of 4 mg *trans*-azobenzene contaminated with an impurity content of 0.3 mol% ($R_1 = R_2 = 391$ K W^{-1}, $R_3 = 110$ K W^{-1}, $R_4 = 108$ K W^{-1}, $C_1 = C_2 = 0.128$ J K^{-1}, $C_3 = 5.6 \times 10^{-3}$ J K^{-1}, $Z = 0.5$). The melting temperature of the eutectic was supposed to be 333 K.

The application of classical methods of purity determination to the curves of Figs. 6–11 should always yield the same impurity concentration because these methods do not take into consideration the variation in the parameters.

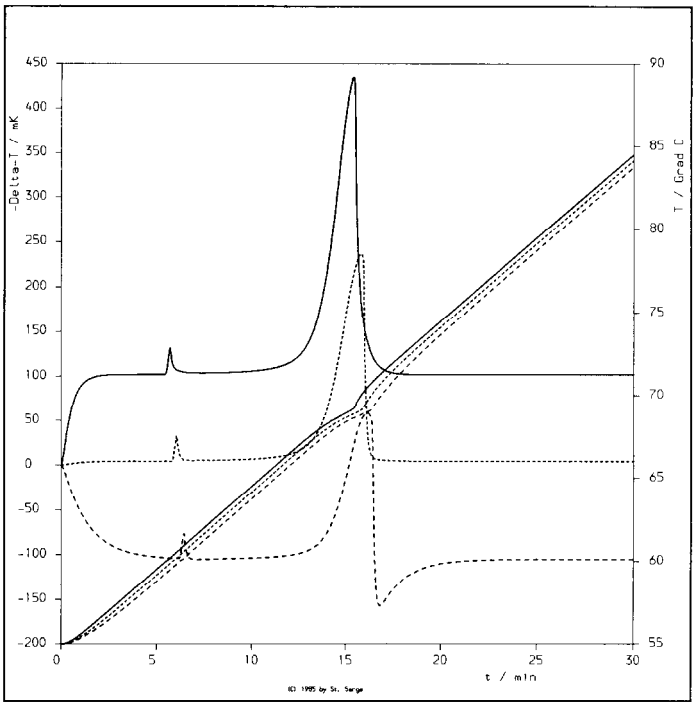

Fig. 6. Variation of R_1 (asymmetry). ———, $R_1 = 130$ K W^{-1}; · · · · · ·, $R_1 = 391$ K W^{-1}; - - - - - -, $R_1 = 1170$ K W^{-1}.

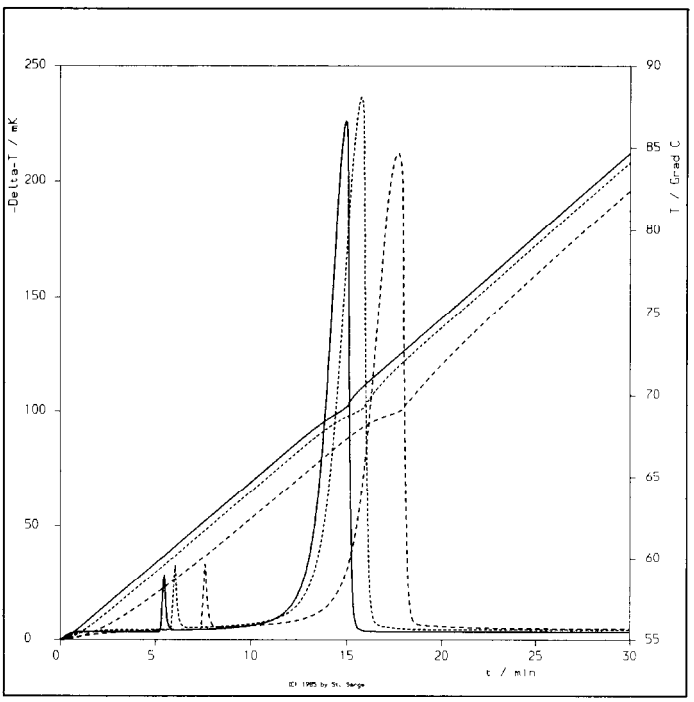

Fig. 7. Variations of R_1 and R_2 (coupling between furnace and sensor). ———, $R_1 = R_2 = 130$ K W^{-1}; · · · · · ·, $R_1 = R_2 = 391$ K W^{-1}; - - - - - -, $R_1 = R_2 = 1170$ K W^{-1}.

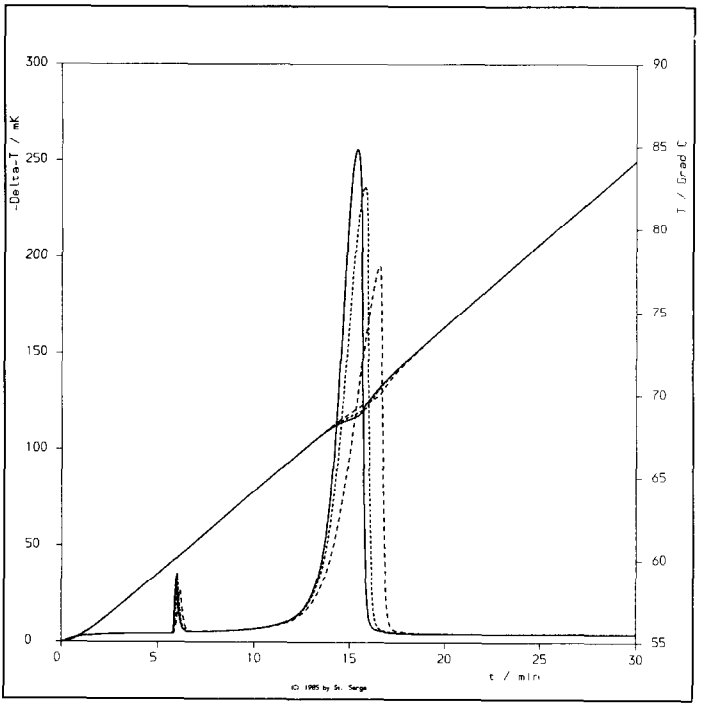

Fig. 8. Variation of R_3 (resistance between sensor and sample). ———, $R_3 = 37$ K W^{-1}; ·····, $R_3 = 110$ K W^{-1}; - - - - - -, $R_3 = 330$ K W^{-1}.

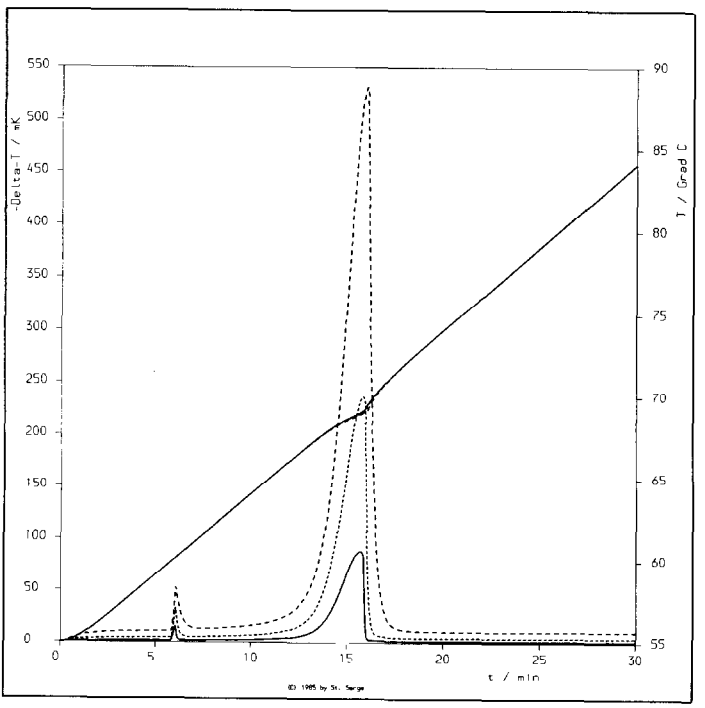

Fig. 9. Variation of R_4 (resistance between sample and reference sensor). ———, $R_4 = 36$ K W^{-1}; ·····, $R_4 = 108$ K W^{-1}; - - - - - -, $R_4 = 324$ K W^{-1}.

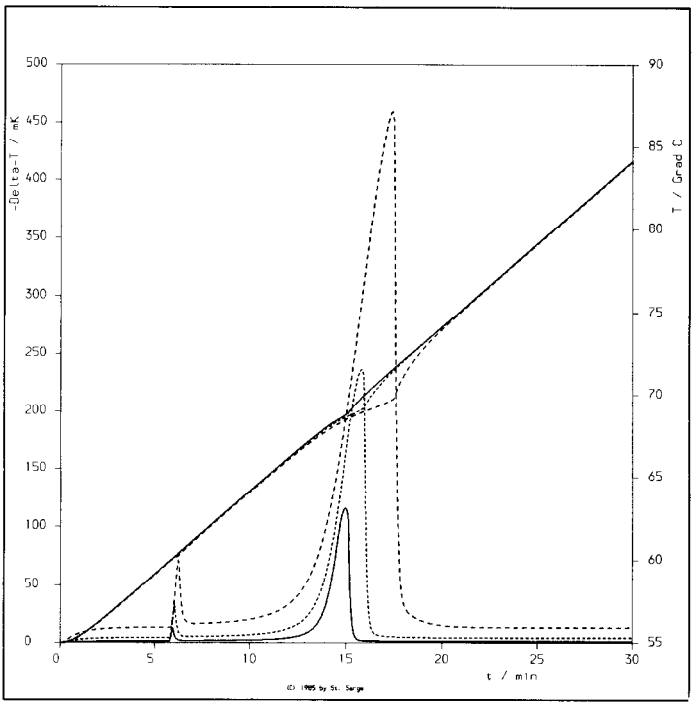

Fig. 10. Variation of C_3 (sample mass). ———, $C_3 = 1.87 \times 10^{-3}$ J K^{-1}; · · · · · ·, $C_3 = 5.60 \times 10^{-3}$ J K^{-1}; - - - - - -, $C_3 = 1.68 \times 10^{-2}$ J K^{-1}.

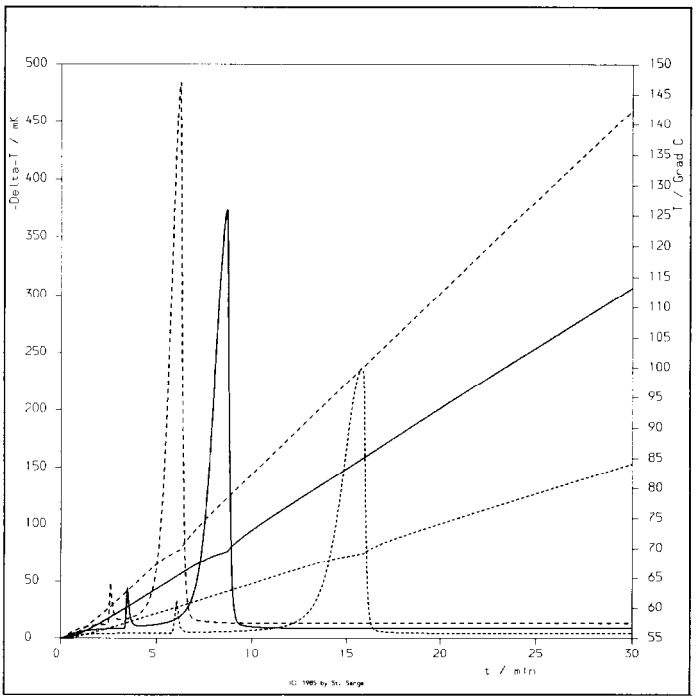

Fig. 11. Variation of β (heating rate). ———, $\beta = 2$ K min^{-1}; · · · · · ·, $\beta = 1$ K min^{-1}; - - - - - -, $\beta = 3$ K min^{-1}.

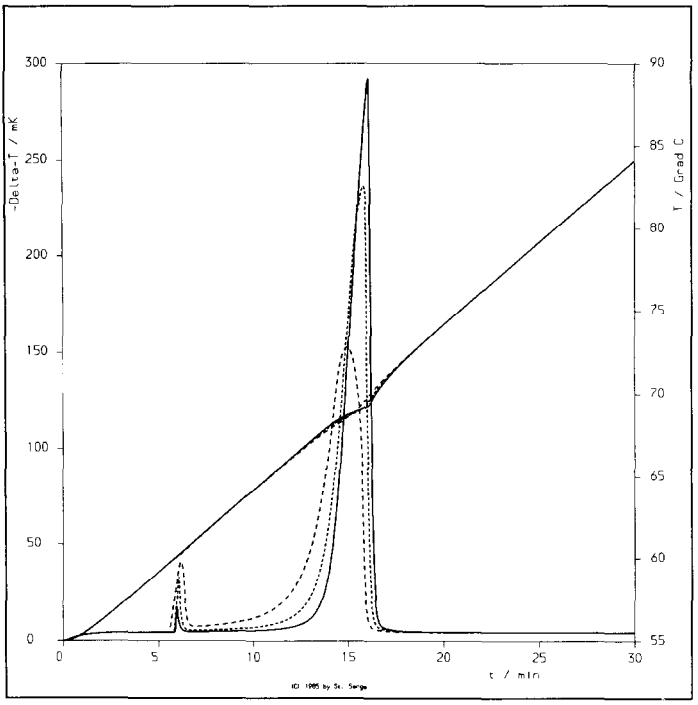

Fig. 12. Variation of $X_2^{\star}$ (impurity concentration). ——, $X_2^{\star} = 0.1$ mol%; · · · · · ·, $X_2^{\star} = 0.3$ mol%; - - - - - -, $X_2^{\star} = 0.9$ mol%.

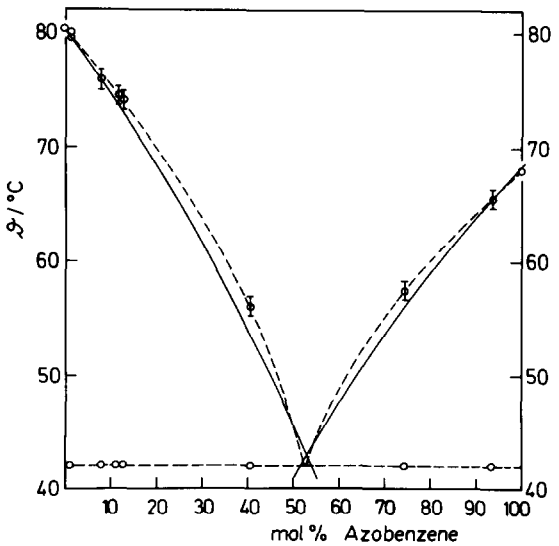

Fig. 13. Phase diagram of naphthalene/*trans*-azobenzene. ——, calculated curve; - - - - - -, experimental curve.

The strong influence of the parameters of the calorimeter and the sample makes evident that classical methods of evaluation have to be modified. Two ways are possible:

1. After the parameters of the calorimeter have been determined, the measured curve is deconvoluted and then evaluated by means of eqn. (10).
2. By means of eqn. (27) a number of enthalpy productions and the corresponding DSC curves are calculated and the deviation between measured and calculated curves is minimized by variation of $X_2^{\star}$.

Now the power of the second method will be discussed:

Naphthalene and *trans*-azobenzene form a eutectic system with $X_{trans\text{-azobenzene}} = 0.52$. Figure 13 shows the experimental phase diagram compared with the theoretically calculated curve: $\Delta_{fus}H^{\ominus}_{naphthalene} = 18.79$ kJ mol^{-1}, $T_{fus,\,naphthalene} = 353.40$ K, $\Delta_{fus}H^{\ominus}_{trans\text{-azobenzene}} = 22.65$ kJ mol^{-1}, $T_{fus,\,trans\text{-azobenzene}} = 341.7$ K, $Cp^{\ominus}_{naphthalene} = 165.5$ J mol^{-1} K^{-1} [5–9].

Two mixtures were prepared from zone-refined material with naphthalene as the main component and with $X_2^{\star} = 0.98$ and 5.01 mol%. For this purpose the starting materials were weighed, melted, mixed, quenched, crushed in a mortar, weighed into DSC pans and the DSC curves recorded.

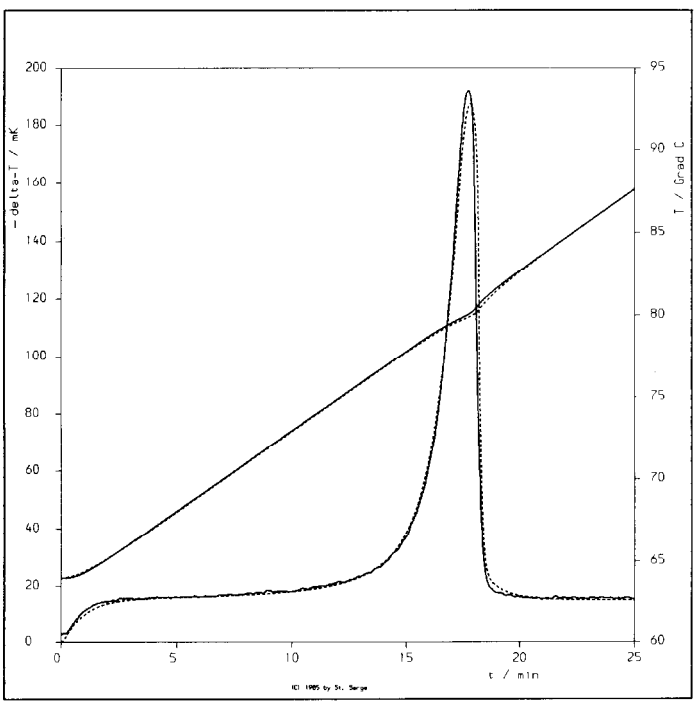

Fig. 14. Measured and calculated melting curve of naphthalene with 0.98 mol% impurity concentration. ———, experimental curve; - - - - - -, simulated curve.

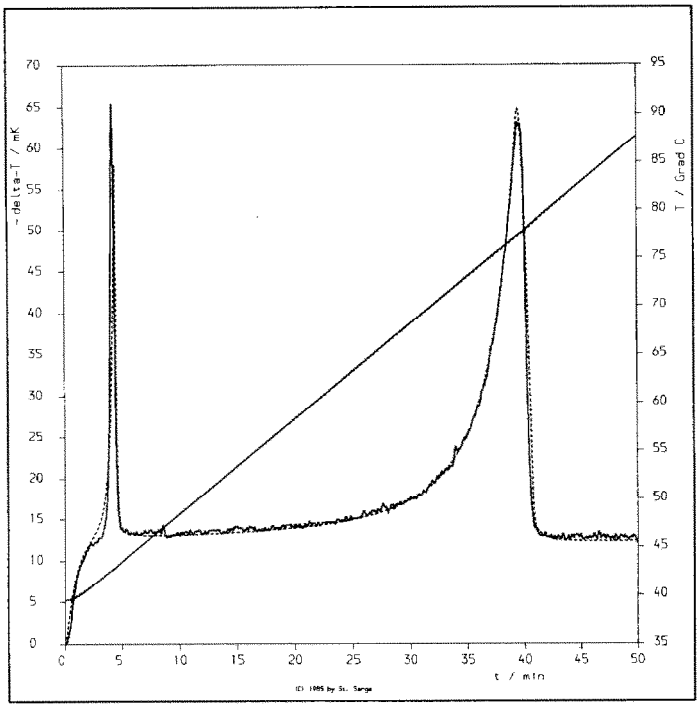

Fig. 15. Measured and calculated melting curve of naphthalene with 5.01 mol% impurity concentration. ———, experimental curve; - - - - - -, simulated curve.

According to the procedure described above for simulating DSC curves, several curves were calculated using the parameters of Table 1. The impurity concentration was varied and the resulting curves were compared with the experimental ones. The criterion for the best fit was the minimum sum of squares of deviations in the ascending parts of the curves. Figures 14 and 15 show the measured curves compared with the calculated curves.

To simplify the comparison between measured and calculated curves, the measured curves were corrected by converting the output of the amplifier under consideration of the Pt 100 curve into a temperature difference $T_1 - T_2$, by correcting the amplifier offset and by temperature calibration.

The minimum deviation between the measured and calculated curves was obtained with $X_2^\star = 0.80$ and 5.40 mol%. This corresponds to an error in the impurity concentration of -18 and $+8\%$.

OUTLOOK

The following projects are to be realized in the near future or have just been undertaken: examination of the naphthalene/*trans*-azobenzene system in the whole range of concentration; examination of a system which forms solid solutions (*trans*-azobenzene/*trans*-stilbene); measurements with other

calorimeters (DuPont 990, Mettler FP 84, Mettler TA 2000); and improvement of the determination of the parameters of the calorimeters and check with independent measurements (e.g. electrical calibration).

LIST OF SYMBOLS

a_{X_i}	activity of component i
β	heating rate
C_i	heat capacity of zone i
$C\mathrm{p}$	heat capacity
F	fraction melted
H	enthalpy
H_{eu}	enthalpy of eutectic
$\Delta_{\mathrm{fus}}H_i$	heat of fusion
$\Delta_{\mathrm{fus}}H_i^{\ominus}$	standard heat of fusion
$\Delta_{\mathrm{mix}}H_i$	heat of mixing
$\mathrm{d}H/\mathrm{d}t$	enthalpy production
k	number of components
K	additional peak area
n_i	number of moles of component i
$\mathrm{d}Q_i/\mathrm{d}t$	heat flux to point i
R	gas constant
R_i	heat resistance of path i
t	time
T	absolute temperature
T_{fus}	temperature of fusion
T_{eu}	temperature of fusion of eutectic
X_i	mole fraction of component i
$X_2^{\star}$	mole fraction of impurity in the original mixture

REFERENCES

1 I. Progogine and R. Defay, Chemische Thermodynamik, VEB Deutscher Verlag für Grundstoffindustrie, Leipzig, 1962, p. 377.
2 E.E. Marti, Thermochim. Acta, 5 (1972) 173.
3 A.A. Raskin, J. Therm. Anal., 30 (1985) 901.
4 J.E. Hunter, III and R.L. Blaine, in R.L. Blaine and C.K. Schoff (Eds.), Purity Determination by Thermal Methods, ASTM STP 838, American Society for Testing and Materials, p. 29.
5 H. Bothe, Dissertation, Technische Universität Braunschweig, 1980, p. 22.
6 K. Ueberreiter and H.-J. Orthmann, Z. Naturforsch. Teil A, 5 (1950) 101.
7 L.H. Ward, J. Phys. Chem., 38 (1934) 761.
8 F.-W. Schulze, H.-J. Petrick and H.K. Cammenga, Z. Phys. Chem. Neue Folge, 107 (1977) 1.
9 H.U.v. Vogel (Ed.), Chemikerkalender, 2nd edn., Springer-Verlag, Berlin, Heidelberg, New York, 1974, p. 570.